Available online at www.sciencedirect.com
ScienceDirect
Journal of the European Ceramic Society 31 (2011) 577–588
www.elsevier.com/locate/jeurceramsoc

Lead free (Li,Na,K)(Nb,Ta,Sb)O_3 piezoelectric ceramics: Influence of sintering atmosphere and ZrO_2 doping on densification, microstructure and piezoelectric properties

G. Lévêque [a], P. Marchet [a,*], F. Levassort [b], L.P. Tran-Huu-Hue [b], J.R. Duclere [a]

[a] *Laboratoire de Sciences des Procédés Céramiques et de Traitements de Surface (SPCTS), UMR 6638 CNRS, Université de Limoges, 12 Rue Atlantis, F-87068 Limoges Cedex, France*

[b] *Université François Rabelais de Tours, UMR Imagerie et Cerveau, – Inserm U 930 – CNRS ERL 3106 10, Boulevard Tonnellé, BP 3223, F-37032 TOURS Cedex 1, France*

Received 26 July 2010; received in revised form 12 October 2010; accepted 27 October 2010
Available online 15 December 2010

Abstract

(Li/Na/K)(Nb/Ta/Sb)O_3 lead free piezoelectric materials (LTLS), "pure" or doped by 1 mass% ZrO_2, were elaborated. The sintering was investigated both by classical way and buried in a powder-bed in order to prevent the alkali-elements losses. The effects of doping and of these processes on densification and piezoelectric properties (d_{33}, k_t and k_p) were studied. The results demonstrated that the final densification is enhanced for ZrO_2 doped samples. The sintering in powder-bed clearly enhanced the piezoelectric properties. The best results corresponds to $d_{33} \approx 180$ pC/N and $k_t \approx 45$–50% for non-doped samples and, $d_{33} \approx 150$ pC/N, with $k_t \approx 45$–50% for ZrO_2 doped samples. Finally, the ultrasonic properties of piezoelectric transducers based upon these materials were also investigated experimentally and theoretically. The results clearly demonstrated that their bandwidth and sensitivity are suitable for use in piezoelectric transducers and comparable with similar PZT based transducers.

Keywords: Niobates; Perovskites; Piezoelectric properties; Functional applications; Ultrasonic-transducers

1. Introduction

Actually, $PbZr_{(1-x)}Ti_xO_3$ (PZT) and lead-based compounds constitute the best family of piezoelectric and ferroelectric materials suitable for integration in devices, such as actuators, sensors and ultrasonic transducers. However, at the present time, there are some restrictions based upon European directives and thus lead-based piezoelectric materials are only tolerated for piezoelectric devices.[1] As a consequence, new lead-free materials are actually the aim of a lot of studies and several recent papers made an inventory of the compounds actually considered as potential candidates for the replacement of PZT.[2–4]

Among the different materials available, the alkali–niobates are considered as very promising. As a consequence, over the past few years, much attention has been given to the lead-free compounds based upon solid solution between $NaNbO_3$ and $KNbO_3$. However, around the composition $K_{0.5}Na_{0.5}NbO_3$ (KNN) their piezoelectric properties are especially interesting because of the occurrence of a morphotropic phase boundary (MPB) similar to the one of PZT.[5] Unfortunately, KNN presents several problems related to sintering and thus, the PZT compounds were preferred because they are easier to elaborate by classical ceramic processes. However, the major drawbacks of KNN ceramics are (i) difficulties in sintering by classical ceramic routes and in the control of the microstructure, (ii) the volatility of alkaline elements and (iii) high sensitivity of the properties to stoichiometry.[6] Similar solid-solutions based upon KNN were also recently investigated or re-investigated, such as KNN–$LiNbO_3$ or KNN–$LiTaO_3$.[7–12] For all of them, a general trend can be evidenced: (i) the evaporation of (at least) one of the alkali constituents of the MPB involve an evolution of the chemical composition and the formation of secondary phases that results in poor properties and (ii) this mechanism is associated with abnormal gain growth, these two phenomena being probably correlated.[13,14]

* Corresponding author. Tel.: +33 5 87 50 23 73; fax: +33 5 87 50 23 07.
E-mail address: pascal.marchet@unilim.fr (P. Marchet).

0955-2219/$ – see front matter © 2010 Elsevier Ltd. All rights reserved.
doi:10.1016/j.jeurceramsoc.2010.10.031

The research in alkali–niobates was recently boosted, since a paper in Nature [15] reported exceptionally high piezoelectric coefficients for textured ceramics prepared by a complex processing method in the system $(Na/K)NbO_3$–$LiTaO_3$–$LiSbO_3$. As for "pure" KNN, this system corresponds to the occurrence of a MPB, with d_{33} values around 370–415 pC/N for textured ceramics, associated to Curie temperatures higher than 250 °C. Examination of the corresponding paper evidenced that interesting properties were also obtained for samples elaborated by a conventional ceramic route: d_{33} higher than 200 pC/N and Curie temperature greater than 200 °C. But this paper is quite short and at the present time, if we compare this system to the lead-containing materials such as PZT (more than 12,000 papers published since 1960), only few data are available concerning this complex perovskite compounds of the $(Li/Na/K)(Nb/Ta/Sb)O_3$ system.[15–26] In addition, even less data are reported about the properties of these materials in real transducer configuration.[27–29] As a consequence, the ceramic process related to this complex system needs to be investigated, in order to verify if they lead to reproducible piezoelectric properties suitable for the elaboration of ultrasonic transducers.

For this purpose, we retained the composition, of global formula $(K_{0,38}Na_{0,52}Li_{0,04})(Nb_{0,86}Ta_{0,1}Sb_{0.04})O_{2,97}$. Indeed, in addition to excellent piezoelectric properties (d_{33} values up to ≈200pC/N) [18], the authors reported that the sintering was easier for this non-stoichiometric composition (K-deficient) than for the stoichiometric one. Unfortunately, they also noticed that the sintering problems are similar to the one observed for "pure" KNN: alkali evaporation associated to the occurrence of a secondary phase of tetragonal tungsten bronze structure (TTB), as for $LiTaO_3$ and $LiNbO_3$ modified KNN.[13,14]

In another way, it was demonstrated for "pure" KNN that doping by ZrO_2 can hinder the exaggerated grain growth.[30] As a consequence, we retained the doping by ZrO_2 as a possible way to solve the sintering problems of such materials. However, the control of the alkali content in such samples is also a key point in order to obtain suitable properties. As a consequence, a method already known for lead containing compounds was also used: some of the $(Li/Na:K)(Nb/Ta/Sb)O_3$ samples were sintered surrounded by a powder bed of the same composition.

Thus, the aim of the present study is (i) to search for the best sintering conditions for ceramics of the abovementioned composition with or without ZrO_2 addition in order to evidence for the role of doping, (ii) for both compositions, to study the effect of sintering atmosphere (powder bed) on the piezoelectric properties and (iii) to test the piezoelectric properties of the best ceramic samples in an ultrasonic transducer configuration.

2. Elaboration and characterization of the samples

As noticed in the introduction, two different compositions were retained for the present study: The first of them was used as a "reference" material and have a the global formula $(K_{0,38}Na_{0,52}Li_{0,04})(Nb_{0,86}Ta_{0,1}Sb_{0.04})O_{2,97}$. It will be hereafter named LTLS. The second one was obtained by adding 1% mass ZrO_2 and will be named as LTLSZ.

Both kind of samples were sintered by two different processes (Table 1): either by a classical way (LTLS and LTLSZ) or covered by LTLS powder which can act as a source of alkaline elements during sintering (LTLSb and LTLZSb) and thus prevents their evaporation. For our best sintering conditions, one sample was also elaborated with only 0.1% mass ZrO_2 (LTLSZc) using the powder bed process, in order to appraise the role of the doping content.

All the samples were elaborated by solid state reaction using high purity (>99%) K_2CO_3, Na_2CO_3, Li_2CO_3, Nb_2O_5, Ta_2O_5, Sb_2O_5 (LTLS, LTLSb) and ZrO_2 (LTLSZ, LTLSZb and LTLSZc). As previously noticed in a recent study concerning the effect of milling process,[31] particle size analysis performed by laser granulometry (Cilas 1064) revealed that the raw materials have very different particle size. As a consequence and in a similar way to this study, the raw materials were first separately ball-milled in ethanol using agate balls, in order to optimize their particle size distribution. After milling, the mean diameters were similar for the different powders (≈1 μm).

As the alkali carbonates are hygroscopic, they were systematically dried at 200 °C for 2 h before using them. All these precursors were then weighted according to the desired composition and homogenized by ball-milling in ethanol during 3 h. The obtained powders were then calcined at 700 °C for 2 h, milled again during 3 h and dried before any use. After reaction and milling, particle size measurement showed a mean diameter around 2 μm. The crystalline phases were checked by X-ray diffraction (Siemens D5000, $\theta/2\theta$ configuration, Cu Kα radiation, rear monochromator).

The obtained powders were then pressed into disks (0.5 tons pressure ≈43 MPa) and sintered at various temperatures ranging from 950 to 1035 °C for 8 h. In order to perform all the characterizations, batches of five pellets were systematically sintered. Then, one of the pellets was crushed and checked by X-ray diffraction. The remaining sintered disks were then rectified in order to obtain parallel surfaces. Their densities were measured both by geometrical measurements and helium pycnometry (Micromeritics AccuPyc 1330).

In order to perform electrical characterization, metallic electrodes were elaborated using platinum paint (Ferro, 6402-1001)

Table 1
Process and composition for the different samples.

Sample name	LTLS	LTLSb	LTLSZ	LTLSZb	LTLSZc
Global formula	$(K_{0,38}Na_{0,52}Li_{0,04})(Nb_{0,86}Ta_{0,1}Sb_{0.04})O_{2,97,}$				
Doping	/	/	1 mass % ZrO_2	1 mass % ZrO_2	0.1 mass % ZrO_2
Sintering	Normal	Powder bed	Normal	Powder bed	Powder bed

sintered at 1000 °C for 30 min. For piezoelectric measurements, the samples were poled at room temperature in silicon oil under DC field (1–7 kV/mm). Piezoelectric constants d_{33} were then measured by a d_{33}-meter (Piezotest PM 300). The electromechanical coupling coefficients (planar and thickness modes) were determined in a first approximation by the measurement of the resonance–antiresonance frequencies (HP4194A impedance analyzer) on the basis of IEEE standards at room temperature.[32] For the best samples, the experimental electrical impedance curves were also fitted with the KLM equivalent electrical Scheme[33] which allows extracting simultaneously dielectric, piezoelectric and mechanical parameters of the corresponding mode.

Finally, the performances of these materials were evaluated in real conditions using a single element transducer and simulations integrating the best ceramic pellets. The experimental results deduced from the electroacoustic response of the transducer were compared with the theoretical behavior (with KLM model). Moreover, a similar transducer, where the piezoelectric element was replaced by a standard PZT, was simulated and its performances were compared to the one obtained for our samples. The results showed the interest of the developed lead-free ceramics for transducer applications.

3. Experimental characterization and discussion

3.1. X-ray diffraction

The calcined powders as well as the sintered pellets were systematically checked by X-ray diffraction (Fig. 1). After the initial calcination of the precursors, X-ray diffraction patterns revealed that: (i) the desired perovskite phase was formed but the diffraction peaks are quite large, which implies probably an imperfect ordering and (ii) a secondary phase, of tungsten–bronze structure (probably $K_3Li_2Nb_5O_{15}$), was also detected. After the sintering, this secondary phase was totally suppressed and only the perovskite phase was evidenced. The occurrence of a similar secondary phase was previously reported for non-stoichiometric samples of the same formula sintered for the same time [18] but contrary to these results, we did not detect the TTB phase after sintering.

For the sintered samples, no noticeable difference was detected between the samples sintered in powder-bed and the other ones, suggesting that the "b" process does not modify drastically the crystalline structure. In order to evidence for the influence of sintering temperature and doping, we selected three samples corresponding to LTLS (1000 and 1035 °C) and LTLSZ sample (1035 °C). A careful examination of the splitting of the pseudo-cubic perovskite peaks indicates that the structure is modified by these two parameters (cf. for example the splitting of the 200 pseudo-cubic, Fig. 1).

For LTLS materials, the room-temperature symmetry was reported as corresponding to a morphotropic phase boundary, associated to the coexistence of both tetragonal and orthorhombic symmetries.[16] An evolution of the symmetry with the sintering time was also demonstrated.[18,26] So, the exact symmetry is difficult to evidence, but the room-temperature X-ray diffraction diagrams correspond more to orthorhombic symmetry, since the 200 peak is splitted in more than two lines (probably three). Another argument for this assumption is the occurrence of two phase transitions above room temperature, as we will see later, which can be attributed respectively to the orthorhombic-tetragonal and tetragonal-cubic phase transitions.[16] So the most probable symmetry at room temperature for the refinement of X-ray diffraction pattern is orthorhombic, even if the occurrence of some tetragonal phase cannot be totally excluded.

Another difficulty in the examination of the diagrams is that the exact space group for the room temperature form is not known. Since the compounds are ferroelectric, they must belong to a non-centrosymmetric point group. As a consequence, for

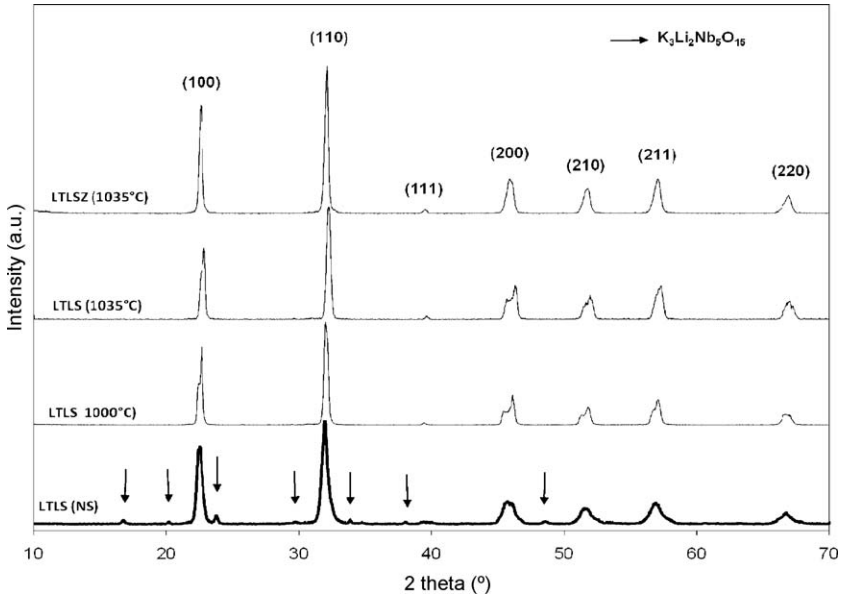

Fig. 1. X-ray diffraction pattern of powder samples: after calcination (LTLS NS), after sintering at 1000 °C (LTLS) and after sintering at 1035 °C (LTLS and LTLSZ 1%ZrO_2). The Miller indices correspond to a pseudo-cubic unit cell and the intensities are in arbitrary units (a.u.).

Table 2
Lattice parameters (calculated by the "pattern matching" method).

Sample	*a* (Å) (±0.0005)	*b* (Å) (±0.0005)	*c* (Å) (±0.0005)	Volume (Å^3)	*b*/*a*	*c*/*a*	*c*/*b*
LTLS1000	3.9453	3.9648	3.9980	62.5	1.005	1.013	1.008
LTLS1035	3.9393	3.9617	3.9928	62.3	1.006	1.014	1.008
LTLSZ1035	3.9449	3.9657	3.9887	62.4	1.005	1.011	1.006

the examination of the evolution of the X-ray diffraction patterns, we retained the Pmm2 space group (non-centrosymmetric group and no diffraction conditions). The calculation of the lattice parameters was performed using the "pattern matching" method using the Fullprof suite (Table 2). As it can be observed, there are only small differences between the three samples and their unit-cell volume remains sensibly constant. The increase of the sintering temperature has only a limited influence (LTLS 1000 °C and LTLS 1035 °C): the "*a*" parameter is a little bit decreased, while the "*b*" and "*c*" parameters are only slightly reduced. If we consider the role of the ZrO_2 doping (LTLS 1035 °C and LTLSZ 1035 °C), a slight increase of the "*a*" and "*b*" parameters is observed, while the "*c*" parameter is clearly decreased. Thus, we can conclude that the Zr^{4+} ion is incorporated into the crystalline lattice (solid solution). As its ionic radius (72 pm in 6 coordination number) is larger than the one of Nb^{5+}, Ta^{5+} (64 pm) and Sb^{5+} (60 pm),[34] the distortion of the BO_6 octahedra (due to the B ions) is reduced by this substitution. If we consider that LTLS materials are similar to lead based materials (PZT) or to $BaTiO_3$, this distortion is directly correlated with ferroelectricity. Thus, this doping will clearly modify the physical properties of these compounds, such as the Curie temperature.

3.2. *Effects of ZrO_2 doping and sintering atmosphere on densification*

Preliminary study of LTLS and LTLSZ by dilatometric measurements (not shown here) showed that the densification starts around ≈900 °C for LTLS and ≈1000 °C for LTLSZ, while the maximum shrinkage rate occurs in the temperature range of 1100–1150 °C for the two compositions. These results are coherent with published results concerning (i) Li doped and Li/Ta-co-doped KNN [10,35] and (ii) (K,Na,Li)(Nb,Ta,Sb)O_3 ceramics elaborated by "classical" ceramic route.[16–19] As a consequence, we studied the effect of sintering temperature between 950 and 1125 °C, since higher temperature resulted in the partial melting of the corresponding pellet.

3.2.1. *Effect of ZrO_2 doping*

For the LTLS samples, which constitute the "reference" series, the best densification occurred for a sintering temperature of ≈1000–1050 °C, but the relative density of the corresponding sample (Fig. 2) was only of 85%, indicating the occurrence of some porosity. For 0.1 mass % ZrO_2 (LTLSZc, 1 point at 1035 °C), the result is similar to the one of LTLS (84% relative density). For LTLS, the maximum value is quite small and lower than the one previously reported for the same composition (≈98%) but the reported results [18] corresponds to samples which were cold-isostatically pressed before sintering, which is not the case for our samples. The densities of our samples measured by helium pycnometry (4.4–4.6 g/cm^3) showed that the "bulk" density, i.e. density of the constituting material, is close to the values measured on powders (≈4.69). This fact indicates that the lack of densification is mostly due to open porosity, as confirmed by the examination of the microstructure by FE–SEM pictures (Fig. 3). Higher sintering temperature (1125 °C) induced the occurrence of "huge" open porosity. Considering the size of the open pores observed here, such phenomenon can be attributed unambiguously to the occurrence of a gaseous phase, probably generated by the evaporation of alkali elements, as already evidenced for Ta modified KNN.[13,14]

For the LTLSZ pellets (1 mass % ZrO_2), the maximum relative density is higher than the one of LTLS batch but only for a narrow range of temperatures (1025–1050 °C) and reaches 95% at 1035 °C (Fig. 2). The effect of ZrO_2 doping on densification is thus clearly evidenced. Similar results were previously reported for unmodified KNN.[30] In this study, the authors detected, for a thin region close to the grain boundaries, the diffusion of zirconium in the perovskite lattice. As a consequence, the substitution of Zr^{4+} for Nb^{5+} induces the occurrence of vacancies in the oxygen sublattice. This substitution has to different effects: (i) the grain growth is impeded and (ii) the occurrence of vacancies increases the diffusion at the grain boundaries and thus promotes the sintering process. A similar effect is probably observed here: the grain-boundaries region is affected by the doping and thus the sintering mechanism is modified and the densification increased.

However, a behavior similar to the one of LTLS series was observed by FE-SEM (Fig. 3): some large open porosity was induced in the pellets for higher temperature sintering (1075 °C). Thus, even if the sintering process is improved by the doping, the evaporation of alkali elements is not impeded, particularly for the high temperatures.

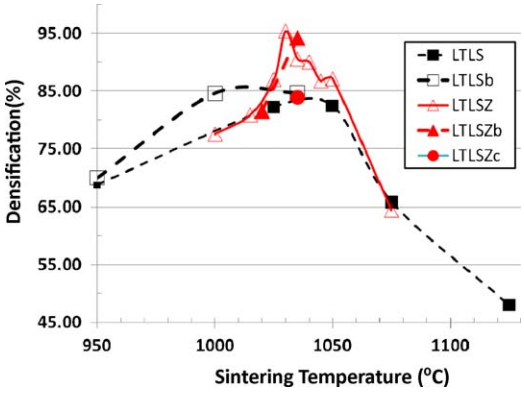

Fig. 2. The relative densities of ceramic pellets (based upon geometrical densities) as a function of sintering temperature.

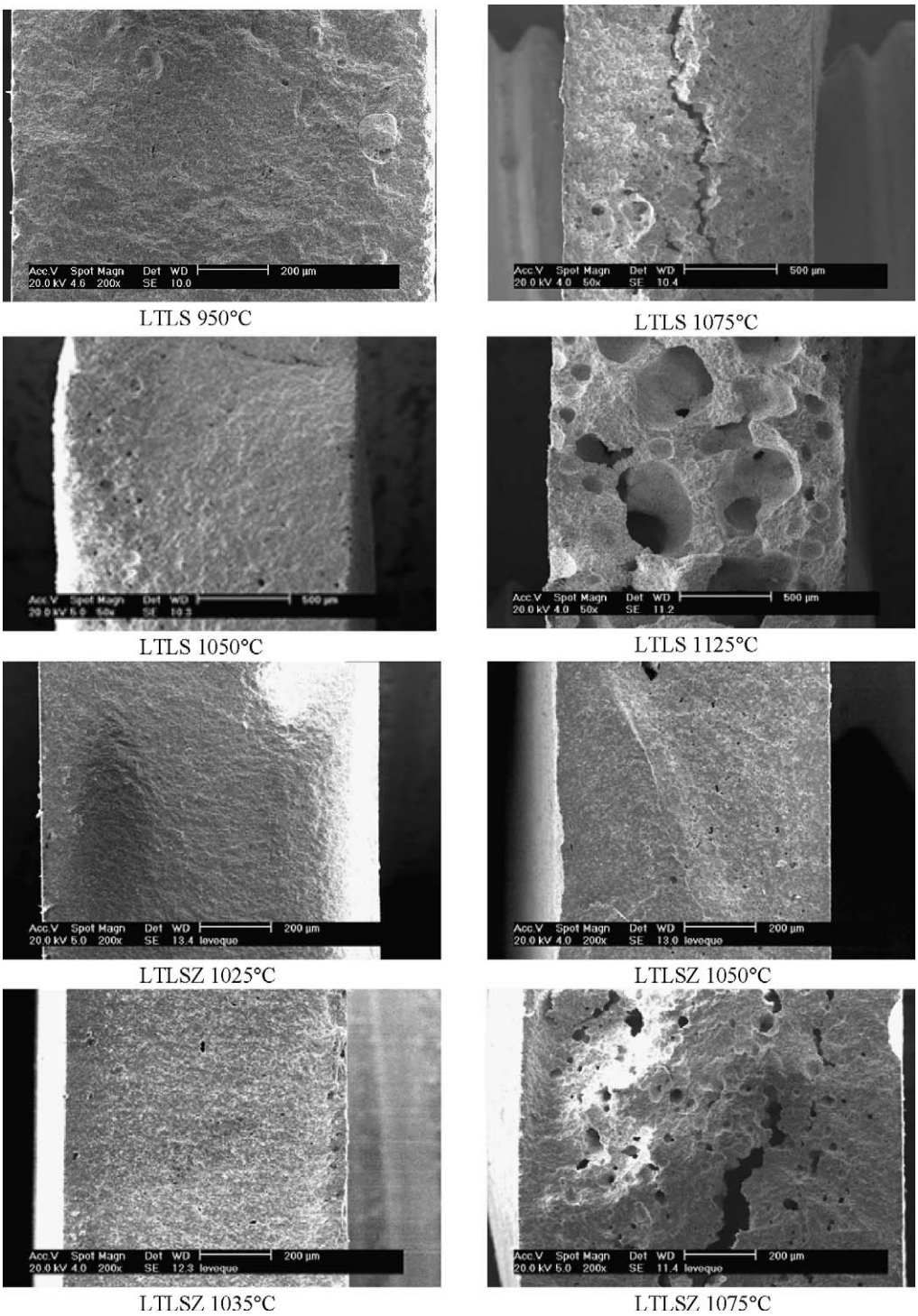

Fig. 3. Microstructures of LTLS and LTLSZ samples for different sintering temperatures (the magnification is different for some samples).

3.2.2. Effect of sintering atmosphere

In order to study the effect of sintering atmosphere on alkali-elements evaporation, some samples were sintered with the green pellets buried in LTLS powder. Such a process generates around the samples an alkali-rich atmosphere which could prevent the alkali losses originating from the pellets. The relative densities of corresponding samples, respectively named LTLSb (3 points) and LTLSZb, sensibly have the same values that the one of LTLS and LTLSZ samples (Fig. 2). So, if this process has an effect, it does not change drastically the final densities of the samples.

3.3. Piezoelectric properties

3.3.1. d_{33} piezoelectric coefficient

Before the measurements, the pellets were poled using a continuous DC voltage applied for 30 min in silicon oil at room temperature, afterward the occurrence of the

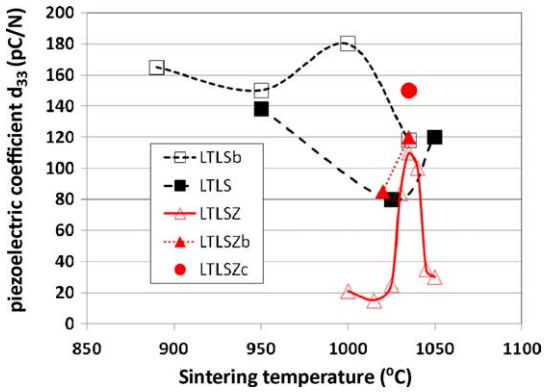

Fig. 4. Evolution of the piezoelectric coefficient d_{33} as a function of sintering temperature.

resonance–antiresonance signal was checked and the d_{33} value measured. This process was repeated up to the occurrence of a d_{33} constant value. Logically, we did not succeed in poling the porous samples sintered at temperatures higher than 1050 °C, since electrical breakdown occurred. For the other samples, the sintering temperature dependence of the d_{33} piezoelectric coefficients for LTLS, LTLSb, LTLSZ and LTLSZb is represented in Fig. 4. Surprisingly, the non-doped samples of the LTLS batch, which presents only poor values of relative density (85% maximum), gave better d_{33} values than for the LTLSZ samples (85–95% relative density).

Considering the role of the sintering atmosphere on piezoelectric properties for non-doped samples, the effect of the "*b*" process is clearly evidenced, since the values obtained by this way are higher than the one obtained for "classical sintering". The best values were obtained for the LTLSb serie and reached 180 pC/N, which is similar to reported values for the same composition (195 pC/N[18]) but lower than the best values reported for this complex system (308 pC/N[16]).

Concerning the 1 mass % ZrO_2 doped samples (LTLSZ samples), the highest value (110pC/N) was obtained for the pellets corresponding to the best sintering temperature (1035–1040 °C, 90–95% relative density). As a matter of comparison, the LTLSZb pellets, which density does not differ from the LTLSZ one, gave higher values of d_{33} (120 pC/N at 1035 °C) using the same polarization conditions (5.5–6 kV/mm). So, as for non-doped samples, preventing the alkali losses by the "*b*" process clearly enhances the d_{33} values.

So, we can suppose that a lower content of ZrO_2 combined with the bed-powder process could be interesting. For this purpose, we prepared a sample (LTLSZc) containing only 0.1 mass % ZrO_2 with the same conditions of sintering (1035 °C – 8 h). In this case, the d_{33} value (150 pC/N) is better than the one of the LTLSZ (110 pC/N) and LTLSZb (120 pC/N), but smaller than the best one obtained for the LTLSb samples (180 pC/N, 1000 °C).

As a consequence, we can extract several information from these results: (i) even if the densification is enhanced by 1 mass % ZrO_2 doping, the corresponding piezoelectric coefficients are not reinforced by this substitution, since our best result (180 pC/N) was obtained for a non-doped sample (ii) the densification by the 'b" process (i.e. green pellets buried in LTLS powder during sintering) resulted in higher piezoelectric coefficients (both for doped or undoped samples) and (iii) properties for the ZrO_2 doped samples, combining the "*b*" process and a 0.1 mass % ZrO_2 gave the best piezoelectric (150 pC/N), but this one are lower than for LTLS samples (180 pC/N).

3.3.2. *Electromechanical coefficients k_t and k_p*

The values of electromechanical coupling factors k_p (planar mode) and k_t (thickness mode) have been first estimated for disk samples using the measurements of electrical impedance as a function of frequency (IEEE standard [32]). For example, to calculate the thickness coupling factor, the following relation was used:

$$k_t = \frac{\pi}{2}.\frac{f_s}{f_p}\tan\left(\frac{\pi}{2}.\frac{f_p - f_s}{f_p}\right)$$

where f_s is the series resonant frequency at which the conductance reaches the minimum and f_p is the parallel resonant frequency at which the resistance reaches the maximum. These results are represented in Fig. 5 as a function of sintering temperature for the five batches. Again, only few results are available for the LTLS samples since they were difficult to pole, but the effect of sintering in powder-bed is again clearly evidenced. This is not the case for the LTLSZb samples (only 2 points): the corresponding coupling coefficients seem to be lower than the one of LTLSZ. In the case of LTLSZc (0.1 mass % ZrO_2), k_t and k_p are similar to the values of LTLZSb for the same temperature.

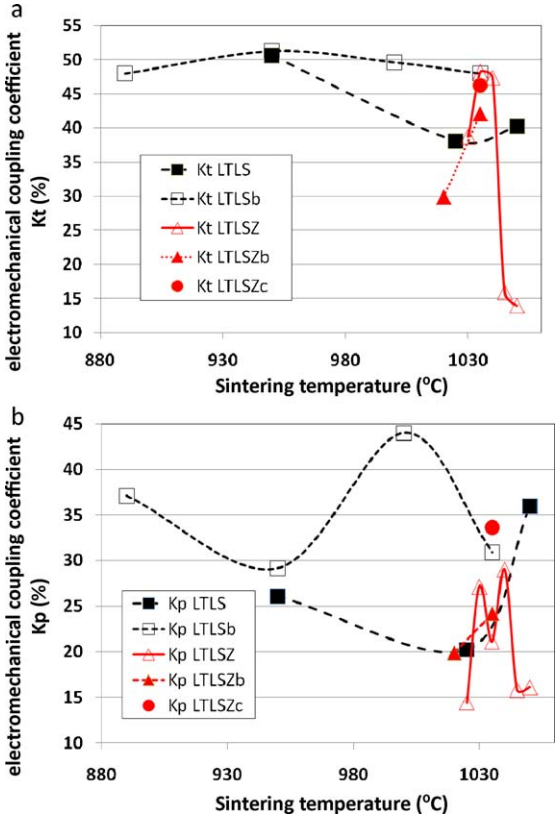

Fig. 5. Evolution of (a) k_t and (b) k_p (IEEE Standard) as a function of sintering temperature.

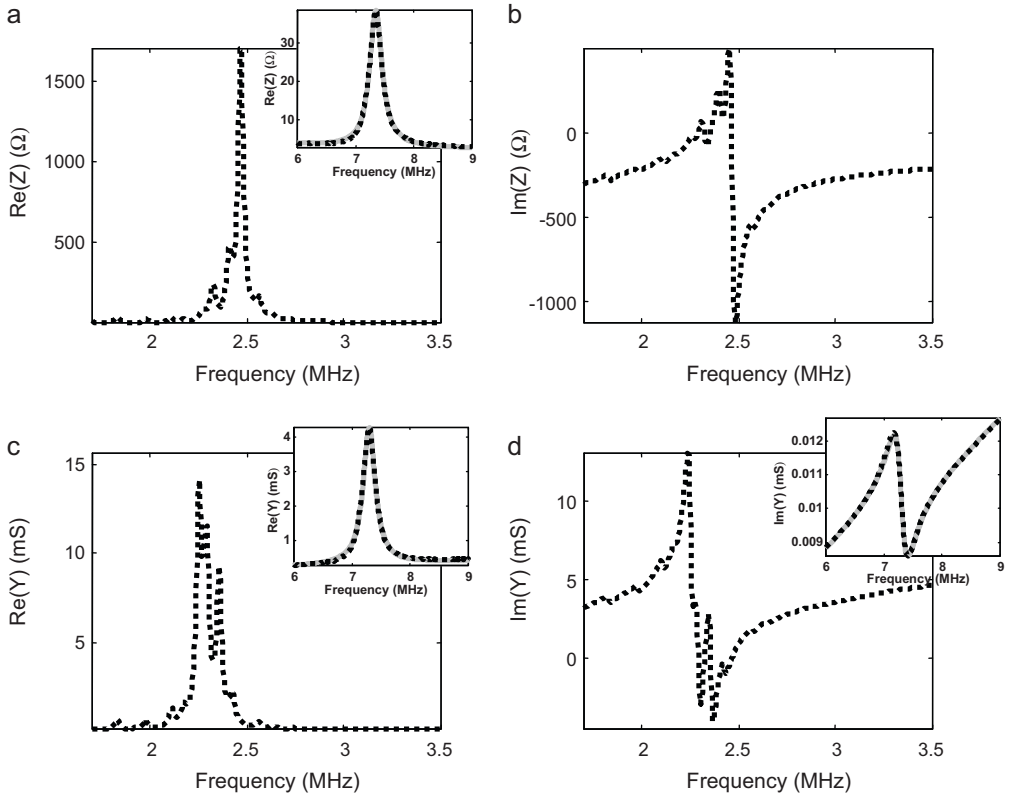

Fig. 6. Experimental complex electrical impedance and admittance of LTLSZc sample (black dashed lines) at fundamental resonance (LTLSZc4 sample, Table 3). In the frames, the first harmonic (experimental: black dashed lines, theoretical: grey solid lines) is represented.

The best values obtained for our samples (IEEE standard) are: for LTLS $k_t \approx 50\%$ and $k_p \approx 35\%$, for LTLSb $k_t \approx 47$–50% and $k_p \approx 45\%$, for LTLSZ $k_t \approx 46$–48% and $k_p \approx 28\%$, for LTLSZc $k_t \approx 50\%$ and $k_p \approx 46\%$.

As shown of Fig. 6, the determinations of the fundamental resonance and antiresonance frequencies are difficult to obtain with accuracy for several samples, where multiple peaks appear in the resonance frequency range. As a consequence, in order to minimize the possible errors on the determination of several related parameters, a complementary characterization was also performed for the best samples (LTLSb, LTLSZb and LTLSZc). This characterization was based on a fitting process of the complex electrical impedance as a function of frequency with the equivalent electrical scheme KLM.[33] Moreover, this characterization allows obtaining dielectric and mechanical losses. To avoid uncertainties on the determination of the parameters (longitudinal wave velocity, anti-resonant frequency, thickness coupling factor and losses), the first overtone is used for the fitting process (as shown in frames in Fig. 6).[36] The thickness of the silver electrodes is in the range 10–60 μm according to the considered samples and has been also taken into account in the calculation of the electrical impedance with the KLM scheme, in order to deduce only the properties of the piezoelectric material. The results for the thickness mode are summarized in Table 3 and compared to a commercial PZT sample. These simulations demonstrate that k_t values determined directly by the first method (from IEEE standards) are overestimated compared to the results obtained with the KLM scheme (method 2): for LTLSb 32–37% against 47–50%, for LTLSZb ≈ 40–42% against 46–48% and finally for LTLSZc ≈ 40–42% against ≈46%. The influence of variations in several parameters such as thickness or electrode area of piezoelectric disks on deduced properties was studied for similar configurations. Results showed that the influence of these variations on extracted parameters of Table 3 were relatively low. In particular for the k_t, the variations have been evaluated around ±1.5%. Details to obtain these possible error values are given in Ref. 37

For the planar mode, the calculation was performed only for the LTLSb samples but the results are similar; the k_p values calculated using the method 1 (40–45%) are also overestimated if compared to the calculated values (38–40%). The conclusion of this study is that (i) the k_p and k_t values of these materials are of the same order of magnitude for both modes (i.e. 35–40%) and (ii) the ZrO_2 doping at low level (0.1 mass %) improve the properties of such materials, which are consequently interesting but lower than the values of k_p and k_t for commercial PZT (for example 59% and 47% for PZ27 Ferroperm [38]).

3.4. Thermal evolution of the properties

3.4.1. Dielectric constant and losses

In order to study the effects of ZrO_2 doping on electrical properties and phase transitions, the dielectric constant, ε_r, and losses, $\tan(\delta)$, were measured as a function of temperature (Fig. 7) for three samples corresponding to increasing ZrO_2 content: LTLSb

Table 3
Piezoelectric characteristics of the ceramic samples (Φ: sample diameter, d_{33}: piezoelectric coefficient, k_{p1} and k_{t1}: planar and thickness coupling factor deduced from the method 1 (from IEEE standard), $\varepsilon_{33}{}^{s}/\varepsilon_0$: dielectric constant at constant strain, c_1: longitudinal wave velocity, k_{t2}: thickness coupling factor deduced from the method 2 (with KLM scheme), f_a: anti-resonant frequency, δ_m: mechanical losses measured at f_a, δ_e: electrical losses measured at f_a, LTLSb5, bold letters: sample used for transducer fabrication).

Sample	Φ (mm)	Relative density (%) (±1)	d_{33} (pC/N) (±5%)	k_{p1} (%)	k_{t1} (%)	$\varepsilon_{33}{}^{s}/\varepsilon_0$	c_1 (m/s)	k_{t2} (%)	f_a (MHz)	Z (MRa)	δ_m (%)	δ_e (%)
LTLSb2	12	84.6	175	44.0	47.6	400	7370	33.5	4.2	28.8	4.9	4.0
LTLSb3	12	84.1	170	40.8	45.4	310	7700	37.3	4.4	29.8	6.8	4.5
LTLSb5	**20**	**78.7**	**175**	**37.7**	**52.5**	**370**	**7150**	**34.4**	**3.9**	**26.2**	**5.2**	**2.4**
LTLSb6	20	79.4	170	39.3	50.3	390	7360	32.0	4.1	27.2	5.7	4.3
LTLSb7	20	82.0	190	37.7	47.4	420	7345	31.9	4.0	27.7	6.6	1.0
LTLSZb5	20	91.9	130	20.7	40.8	545	6040	21.6	2.8	23.1	5.0	4.0
LTLSZb2	12	91.0	145	24.2	42.1	600	5915	24.3	2.9	25.2	6.8	2.7
LTLZc4	12	83.9	140	32.9	46.5	260	5485	40.2	2.7	20.2	3.6	2.7
LTLSZc5	20	82.2	150	33.6	50.2	230	5415	41.8	2.7	19.9	5.8	3.0
PZ27 Ferroperm [37]	/	/	425	59.2	47	914	3906	47	/	30	/	1.7

(0% ZrO_2), LTLSZc (0.1 mass % ZrO_2) and LTLSZb (1 mass % ZrO_2). All the curves look quite similar and present two anomalies, corresponding respectively to the orthorhombic – tetragonal (≈60–70 °C) and tetragonal – cubic phases transitions (≈375 °C for LTLSb).[16]

The ZrO_2 doping have different consequences on the dielectric anomalies: (i) the Curie point is depressed (375 °C → 345 °C → 290 °C), together with a similar decrease of corresponding anomalies for the tan(δ) curves (ii) the value of the dielectric constant at the maximum of the phase-transition peak is decreased and the corresponding peak is enlarged (iii) the Curie constant (measured at 1 kHz) is also modified: $C = 1.82 \times 10^5$ K^{-1} for LTLSb, $C = 1.78 \times 10^5$ K^{-1} for LTLZc and $C = 2.29 \times 10^5$ K^{-1} for LTLSZb and (iv) the amplitude of the dielectric anomaly close to room temperature is reduced while the value of the dielectric constant at room temperature is increased of ≈20–25%. Such modifications clearly correspond to a structural change and confirm that the Zr^{4+} ion is incorporated into the crystalline lattice, as we previously observed by X-ray diffraction. As for other perovskite systems, the substitution by a larger ion induces a decrease of the amplitude of the peak associated to the ferroelectric – paraelectric phase transition, together with an enlargement of this peak.[5,39]

In addition, the dielectric losses at room temperature are also modified: the 0.1 mass % ZrO_2 addition (LTLSZc) increased the value of tan(δ), while for the 1 mass % ZrO_2 sample (LTLSZb), the value is lower than for undoped-material, probably because the temperature of the orthorhombic – tetragonal phase transition is also modified by the Zr^{4+} addition.

However, the modifications observed here confirm that the Zr^{4+} ion is incorporated into the crystalline lattice, as we previously observed by X-ray diffraction.

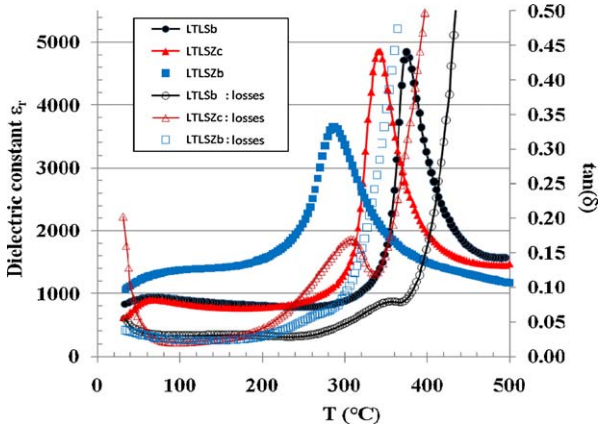

Fig. 7. Evolution of the dielectric constant and dielectric losses as a function of temperature (black circles: LTLSb undoped, red triangles: LTLSZc 0.1 mass % ZrO_2 and blue squares: LTLSZb 1 mass % ZrO_2). (For interpretation of references to color in this figure legend, the reader is referred to the web version of this article.).

3.4.2. Electromechanical coupling coefficients

In order to obtain some information concerning the evolution of the piezoelectric properties between room temperature and Curie temperature, the evolution of the resonance–antiresonance curves for thickness and radial mode was measured. The corresponding coupling coefficients were then calculated (first method) for two samples: LTLSb (undoped material) and LTLSZb sample (1 mass % ZrO_2). The results are represented Fig. 8. As for the dielectric constant, two anomalies are observed: The first one, around ≈50 °C, corresponds to a decrease of the

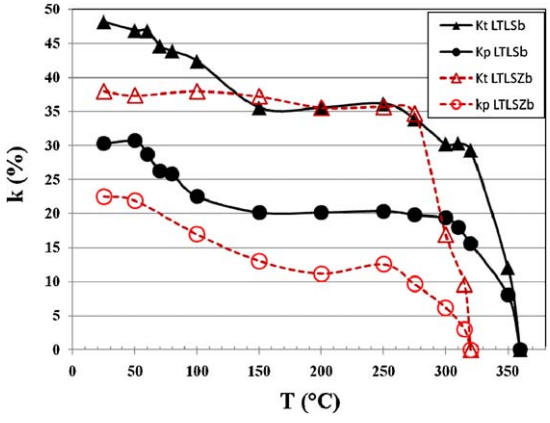

Fig. 8. Evolution of k_p and k_t with temperature for LTLSb sample (sintered at 1000 °C) and LTLSZb samples (sintered at 1035 °C).

coupling coefficients and is associated to the orthorhombic – tetragonal phase transition. The second one corresponds to the disappearing of the polar behavior of the ferroelectric material at the Curie temperature.

For the undoped sample, the variation of both coupling coefficients is quite large at the first phase transition but a value of ≈35% was still obtained for k_t at 250 °C.

In we consider the doped samples and as previously noticed for the dielectric properties: (i) the amplitude of the first anomaly is reduced by the ZrO_2 doping and (ii) the Curie temperature is lowered. For the planar mode, as slow decrease of the coupling coefficient was noticed but a value of ≈13% was still obtain at 250 °C. For the thickness mode, the coupling coefficient remains at sensibly constant level (≈35%) up to 280 °C which is only 70 °C below the Curie temperature.

As a consequence, the stability of the thickness mode is enhanced by this doping, even if the value of k_p is lower than for "pure" material: the k_t value varies only from ≈38% at room temperature to ≈36% at 250 °C. Since the thickness mode is the one which is used for ultrasonic transducers, such a stability of the coupling coefficient is particularly interesting. Indeed, an empirical law generally used for piezoelectronic devices considers that ferroelectric ceramic materials can only be used up to ≈100 °C below their Curie temperature, because of the rapid decrease of the polarization close to the Curie point. Here, the stability range is extended close to Curie temperature in a more efficient way than previously reported.[22,23]

4. Single element transducers

4.1. Transducer fabrication and characterization

For an evaluation of the performances of these materials in conditions of use, a single element transducer was manufactured using one sample of the LTLSb batch (LTLSb5 sample, Table 3). The backing was fabricated with an epoxy resin loaded with tungsten particles. It was directly molded and polymerized on the lead-free piezoelectric disk. No matching layer was added in the front face. This structure was integrated into isolated housing. A coaxial cable with a characteristic impedance of $Z = 50\ \Omega$ was used for the electrical connection to the generator (Fig. 9). The pulse echo response was measured in a water tank on a metallic target at 3 cm and represented with the corresponding frequency response in Fig. 10.

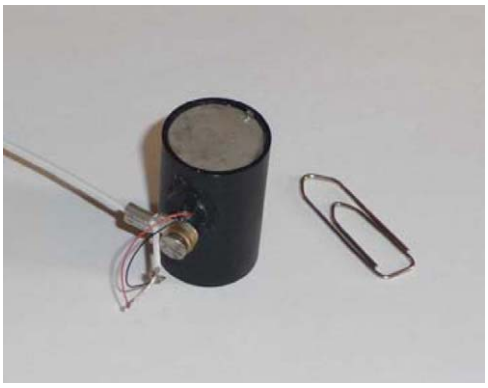

Fig. 9. Picture of the elementary transducer integrating the LTLSb sample (LTLSb5 sample, Table 3).

4.2. Transducer simulations and discussion

The experimental electro-acoustic response was then compared with the one obtained theoretically using the KLM scheme. For this, the data of the piezoelectric element (Table 3) and an acoustical impedance of the backing of 16 MRa were used (Fig. 11). The characteristics are summarized Table 4. Theoretical and experimental results are in good agreement.

Similar theoretical configurations with the KLM equivalent electrical scheme were used to simulate the behavior of single element transducers with different piezoelectric elements. These simulations will allow situating the efficiency of lead-free piezo-

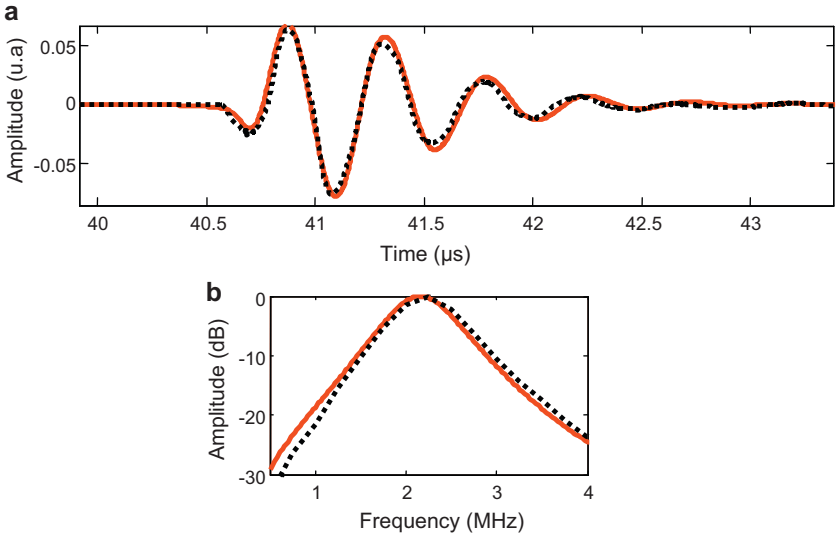

Fig. 10. (a) Experimental (black dashed line) and theoretical (red solid line) electro-acoustic responses; (b) corresponding normalized frequency responses of the LTLSb sample based transducer (For interpretation of references to color in this figure legend, the reader is referred to the web version of this article.).

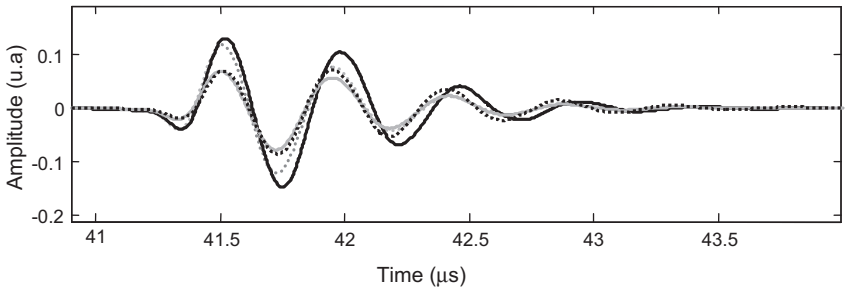

Fig. 11. Simulated electro-acoustic time responses of transducers (LTLSb: grey solid line, standard PZT: Black solid line, modified PZT: black dashed line, LTLSZc: grey points).

electric materials developed here, in comparison with standard piezoelectric materials such as PZT. To have comparable results with the previous simulation, the thickness of the piezoelectric element was adapted to keep a resonant frequency at 2.2 MHz. Moreover, the area of the piezoelectric element was modified to obtain the same electrical impedance values at the resonance frequency (depending mainly of the dielectric constant of the piezoelectric material). This allowed in a 50 Ohm electrical matching to have comparable results in terms of transducer sensitivity. The acoustical impedance of the backing is unchanged at 16 MRa. A standard PZT (Pz27) was used as a reference,[37] but in a first simulation, the k_t was artificially decreased at the same value as the one of the sample LTLSb (34.4%). This is the only change in all the data of the Pz27. Characteristics of the corresponding electro-acoustic response showed that the sensitivity and bandwidth are comparable in both cases. The electroacoustic responses of these different simulations are given in Fig. 11.

Table 5 gives the simulated transducer characteristics. When the right value of k_t is used for the Pz27 (47%), the corresponding configuration delivered the highest characteristics with a sensitivity of 5.6 dB higher than the lead-free transducer (LTLSb) but the bandwidth is comparable, essentially due to slightly higher acoustic impedance for the PZT that for the LTLSb sample. Finally, the fabricated sample with the highest k_t obtained (LTLSZc5 with $k_t = 41.8\%$) was also used to simulate a final configuration. The results showed that this material becomes competitive with the PZT. The sensitivity is relatively closed but due to a lower acoustical impedance (due to material composition but also the porosity content), the bandwidth is higher. As a consequence, this material appears as very promising for the future development of lead-free piezoelectric materials for ultrasonic transducers. Several works have already published with KNN based compositions where single element transducers have been fabricated, evaluated and compared to PZT-based transducer.[27,28] Comparison between these results are difficult (for example depending of the choice of acoustical impedance of the backing), but similar conclusion are given between the lead-free and PZT based transducers, even if any sensitivity value is given. Moreover, the lead-free ceramic has a relatively high longitudinal wave velocity making it especially suitable for high frequency transducer applications.[29]

Table 4
Characteristics of the experimental transducer based upon LTLSb (f_c = center frequency of the response, BP (−6 dB) = bandwidth at −6 dB, BP (−20 dB) = bandwidth at −20 dB).

Sample LTLSb5	f_c (MHz)	BW (−6 dB) (%)	BW (−20 dB) (%)
Experimental	2.2	45	110
Theoretical	2.2	45	115

Table 5
Characteristics of the simulated transducers (k_t: value of thickness coupling factor chosen for each simulation; Z: acoustical impedance of each piezoelectric material; A_{max}: normalized maximum sensitivity (at f_c) (in comparison with transducer using the Pz27 data); BW (−6 dB): relative bandwidth at −6 dB; BW (−20 dB): relative bandwidth at −20 dB).

Sample	k_t (%)	Z (MRa)	A_{max} (dB)	BW (−6 dB) (%)	BW (−20 dB) (%)
LTLSb5 "modified"	34.4	26.0	−5.6	45	118
Pz27	34.4	30.0	−4.7	39	104
Pz27	47.0	30.0	0	47	120
LTLSZc5	41.8	19.9	−1.7	55	134

5. Conclusion

The aim of this study was (i) to search for the best sintering conditions for (Li/Na/K)(Nb/Ta/Sb)O_3 ceramics, with or without ZrO_2 addition, (ii) for both compositions, to study the effects of sintering atmosphere (powder bed) on the piezoelectric properties and (iii) to test the piezoelectric properties of the best ceramic samples in a transducer configuration.

Concerning the ceramic process, we demonstrated that the densification is improved by ZrO_2 doping, but does not prevent the evaporation of alkali elements, as "huge" porosity was observed for high sintering temperature both for doped or non-doped samples. The interest of sintering the pellets in powder-bed was also studied: no noticeable difference was detected in the relative densities of samples sintered at the same temperature with or without powder-bed process. However, the effect of powder-bed process was clearly evidenced on the piezoelectric properties: the values of d_{33} and coupling coefficients k_t and k_p are clearly enhanced when compared to samples sintered by "normal" process.

The interest of a limited addition of ZrO_2 (0.1 mass %) was also evidenced: the d_{33} value of the corresponding sample LTLSZc (150 pC/N) is lower than the one of "pure" LTLSb sintered by the powder-bed process, but the values of k_t coefficients (40–45%), which are the most important parameters for

transducers used in thickness mode, clearly have the same order of magnitude than the one of non-doped samples (45–50% for the best samples). In addition, even if k_t coefficients are a little bit lower than the one of non-doped samples (45–50% for the best samples), their thermal stability is enhanced since the ZrO_2 doping reduces the evolution due to the phase transition close to room temperature.

The experiments and simulations performed on transducers based upon these materials clearly showed that they are very interesting for devices elaboration (competitive with the PZT), particularly the 0.1 mass % doped sample: even if d_{33} and k_t values are lower than the one of commercial PZT, main characteristics of transducers integrating these materials are comparable or higher than in the case of PZT based-transducers. The main explanation of this high performance is found in the acoustical impedance value which is lower than the PZT. The acoustical adaptation between the transducer and the propagation medium (typically water) is naturally improved in this case. The density of this class of materials (3700–3900 kg/m^3) is lower than the one of PZT ($\approx$7700 kg/m^3). This fact alone is an advantage since the weight of the devices could be reduced compared to the PZT based devices. As a second consequence of this reduced density, the velocity of the ultrasonic wave is enhanced (5400–7700 m/s) compared to the PZT values (3900 m/s). This value is also interesting: same thickness of the piezoelectric element will induce a higher resonance frequency, allowing the device to be operated at higher frequency than for a PZT ceramic.

So we can conclude that this class of lead-free materials is very promising for the replacement of PZT in piezoelectronic devices and will probably be intensively investigated in the future, even if a lot of problems related to ceramic process must be resolved before their use in commercial applications.

Acknowledgements

We gratefully thanks the "Delegation Generale de l'Armement" (DGA) which totally supported this work under contract 06 34 055

References

1. Directive 2002/95/EC, On the restriction of the use of certain hazardous substances in electrical and electronic equipment, Official Journal of the European Union 13-02-2003.
2. Demartin Maeder M, Damjanovic MD, Setter N. Lead free piezoelectric materials. *J Electroceram* 2004;**13**:385–92.
3. Rodel J, Kounga ABN, Weissenberger-Eibl M, Koch D, Bierwisch A, Rossner W, Hoffmann MJ, Danzer R, Schneider G. Development of a roadmap for advanced ceramics, 2010–2025. *J Eur Ceram Soc* 2009;**29**:1549–60.
4. Rodel J, Jo W, Seifert KTP, Anton E, Granzow T, Damjanovic D. Perspective on the development of lead-free piezoceramics. *J Am Ceram Soc* 2009;**92**:1153–77.
5. Jaffe B, Cook Jr WR, Jaffe H. *Piezoelectric ceramics*. Academic Press; 1971.
6. Matsubara M, Yamaguchi T, Sakamoto W, Kikuta K, Yogo T, Hirano S. Processing and piezoelectric properties of lead-free (K,Na) $(Nb,Ta)O_3$ ceramics. *J Am Ceram Soc* 2005;**88**:1190–6.
7. Guo Y, Kakimoto K, Ohsato H. Phase transitional behavior and piezoelectric properties of $(Na_{0.5}K_{0.5})NbO_3$–$LiNbO_3$ ceramics. *Appl Phys Lett* 2004;**85**:4121–3.
8. Hollenstein E, Davis M, Damjanovic D, Setter N. Piezoelectric properties of Li- and Ta-modified $(K_{0.5}Na_{0.5})NbO_3$ ceramics. *Appl Phys Lett* 2005;**87**:182905.
9. Guo Y, Kakimoto K, Ohsato H. $(Na_{0.5}K_{0.5})NbO_3$–$LiTaO_3$ lead-free piezoelectric ceramics. *Mater Lett* 2005;**59**:241–4.
10. Saito Y, Takao H. High performance lead-free piezoelectric ceramics in the $(K,Na)NbO_3$–$LiTaO_3$ solid solution system. *Ferroelectrics* 2006;**338**:17–32.
11. Klein N, Hollenstein E, Damjanovic D, Trodahl HJ, Setter N, Kuball M. A study of the phase diagram of $(K,Na,Li)NbO_3$ determined by dielectric and piezoelectric measurements, and Raman spectroscopy. *J Appl Phys* 2007;**102**:014112.
12. Dai Y, Zhang X, Zhou G. Phase transitional behavior in $K_{0.5}Na_{0.5}NbO_3$–$LiTaO_3$ ceramics. *Appl Phys Lett* 2007;**90**:262203.
13. Wang Y, Damjanovic D, Klein N, Hollenstein E, Setter N. Compositional inhomogeneity in Li- and Ta-modified $(K, Na)NbO_3$ ceramics. *J Am Ceram Soc* 2007;**90**:3485–9.
14. Wang Y, Damjanovic D, Klein N, Hollenstein E, Setter N. High-temperature instability of Li- and Ta-modified $(K,Na)NbO_3$ piezoceramics. *J Am Ceram Soc* 2008;**91**:1962–70.
15. Saito Y, Takao H, Tani T, Nonoyama Y, Takatori K, Nomma T, Nagaya T, Nakamura M. Lead-free piezoceramics. *Nature* 2004;**432**:84–7.
16. Ming BQ, Wang JF, Qi P, Zang GZ. Piezoelectric properties of (Li,Sb,Ta) modified $(Na,K)NbO_3$. *J Appl Phys* 2007;**10**:054103.
17. Li E, Kakemoto H, Wada S, Tsurumi T. Influence of CuO on the structure and piezoelectric properties of the alkaline niobate-based lead-free ceramics. *J Am Ceram Soc* 2007;**90**:1787–91.
18. Rubio-Marcos F, Ochoa P, Fernandez JF. Sintering and properties of lead-free $(K,Na,Li)(Nb,Ta,Sb)O_3$ ceramics. *J Eur Ceram Soc* 2007;**27**:4125–9.
19. Chang Y, Yang Z, Xiong L, Liu Z, Wang Z. Phase structure, microstructure, and electrical properties of Sb-modified (K, Na,Li) $(Nb, Ta)O_3$ piezoelectric ceramics. *J Am Ceram Soc* 2008;**91**:2211–6.
20. Ochoa DA, Garcia JE, Perez R, Gomis V, Albareda A, Rubio-Marcos F, Fernandez JF. Extrinsic contribution and non-linear response in lead-free KNN-modified piezoceramics. *J Phys D Appl Phys* 2009;**42**:025402.
21. Rubio-Marcos F, Navarro-Rojero MG, Romero JJ, Marchet P, Fernandez JF. Piezoceramics properties as a function of the structure in the system $(K,Na,Li)(Nb,Ta,Sb)O_3$. *IEEE T Ultrason Ferr* 2009;**56**:1835–42.
22. Fu J, Zuo R, Wang X, Li L. Phase transition characteristics and piezoelectric properties of compositionally optimized alkaline niobate based ceramics. *J Alloy Compd* 2009;**486**:790–4.
23. Zuo R, Fu J, Lv D. Phase transformation and tunable piezoelectric properties of lead-free $(Na_{0.5}2K_{0.48-x}Li_x)(Nb_{1-x-y}Sb_yTa_x)O_3$ system. *J Am Ceram Soc* 2009;**92**:283–5.
24. Lin D, Kwok KW, Chan Lai-Wa H. Effect of alkali elements content on the structure and electrical properties of $(K_{0.48}Na_{0.48}Li_{0.04})(Nb_{0.90}Ta_{0.04}Sb_{0.06})O_3$ lead-free piezoelectric ceramics. *J Am Ceram Soc* 2009;**92**:2765–7.
25. Fu J, Zuo R, Lv D, Liu Y, Wu Y. Structure and piezoelectric properties of lead-free $(Na_{0.52}K_{0.442x})(Nb_{0.952x}Sb_{0.05})O_{3-x}LiTaO_3$ ceramics. *J Mater Sci: Mater El* 2010;**21**:241–5.
26. Rubio-Marcos F, Marchet P, Merle-Mejean T, Fernandez JF. Role of sintering time, crystalline phases and symmetry in the piezoelectric properties of lead-free KNN-modified ceramics. *Mater Chem Phys* 2010;**123**:91–7.
27. Hagh NM, Jadidian B, Ashbahian E, Safari A. Lead-free piezoelectric ceramic transducer in the donor-doped $K_{1/2}Na_{1/2}NbO_3$ solid solution system. *IEEE Trans Ultrason Ferr* 2008;**55**:214–24.
28. Safari A, Abazari M, Kerman K, Maradian-Hagh N, Koray Akdogan EK. $(K_{0.44}Na_{0.52}Li_{0.04})(Nb_{0.84}Ta_{0.10}Sb_{0.06})O_3$ ferroelectric ceramics. *IEEE Trans Ultrason Ferr* 2009;**56**:1586–94.
29. Wu DW, Chen RM, Zhou QF, Shung KK, Lin DM, Chan HLW. Lead-free KNLNT piezoelectric ceramics for high-frequency ultrasonic transducer application. *Ultrasonics* 2009;**49**:395–8.
30. Malic B, Bernard J, Bencan A, Kosec M. Influence of zirconia addition on the microstructure of $K_{0.5}Na_{0.5}NbO_3$ ceramics. *J Eur Ceram Soc* 2008;**28**:1191–6.
31. Rubio-Marcos F, Romero JJ, Martin-Gonzalez MS, Fernandez JF. Effect of stoichiometry and milling processes in the synthesis and the piezoelectric

properties of modified KNN nanoparticles by solid state reaction. *J Eur Ceram Soc* 2010;**30**:2763–71.
32. ANSI/IEEE Standard on Piezoelectricity. *IEEE Trans Ultrason Ferr* 1996;43:717–718.
33. Krimholt K, Leedom DA, Matthaei GL. New equivalent circuits for elementary piezoelectric transducers. *Electron Lett* 1970;**38**:398–9.
34. Shannon RD. Revised effective ionic radii and systematic studies of interatomic distances in halides and chalcogenides. *Acta Cryst* 1976;**A32**:751–67.
35. Zhen Y, Li JF. Normal sintering of (K,Na)NbO_3-based ceramics: influence of sintering temperature on densification, microstructure, and electrical properties. *J Am Ceram Soc* 2006;**89**:3669–75.
36. Tran-Huu-Hue LP, Levassort F, Lethiecq M, Certon D, Patat F. Characterization of the piezoelectric and dielectric relaxation parameters of 0–3 composites and PVDF materials in thickness mode. *Ultrasonics* 1997;**35**:317–24.
37. Bardaine A, Boy P, Belleville P, Acher O, Levassort F. Improvement of composite sol–gel process for manufacturing 40 microns piezoelectric thick films. *J Eur Ceram Soc* 2008;**28**:1649–55.
38. http://www.ferroperm-piezo.com.
39. Gomah-Pettry JR, Marchet P, Simon A, Von Der Mühll R, Maglione M, Mercurio JP. Dielectric properties of $Na_{0.5}Bi_{0.5}TiO_3$ – $BaTiO_3$ ceramics. *Integr Ferroelectr* 2004;**61**:159–62.